

## CHAPTER IV

### RESULTS AND DISCUSSION

Polyhydroxyalkanoates (PHA), a new class of biopolymers, have been found to be synthesized by many bacterial strains as an intracellular carbon and energy storage compound. PHAs are generally biodegradable, with good biocompatibility, making them logical choices for uses in various biomedical applications. In spite of the fact that over 90 different types of PHA consisting of various monomers have been reported, only few of them are studied for this purpose (Zinn *et al.*, 2001). So far, poly 3-hydroxybutyrate (PHB), copolymers of 3-hydroxybutyrate and 3-hydroxyvalerate (PHBV), poly 4-hydroxybutyrate (P4HB), copolymers of 3-hydroxybutyrate and 3-hydroxyhexanoate (PHBHHx), and poly 3-hydroxyoctanoate (PHO) are available in sufficient quantity for applicable research. The *in vitro* study of biocompatible PHB and PHBV fabricated by both casting film and solute-leaching technique has been widely reported with various cell lines, including osteoblasts, epithelial cells and ovine chondrocytes (Rivard *et al.*, 1996). Additionally, cells of various origins cultured on PHB and PHBV films exhibited high levels of cell adhesion. The investigation showed that these materials can be used to make matrices for *in vitro* proliferous cells; plus, the investigated properties of PHB and PHBV films proved to be fundamentally similar (Shishatskaya *et al.*, 2004). However, the fragility of PHB is the main drawback that restricts its application. Such a drawback can be optimized by blending or by selecting the appropriated PHA, and therefore, this work was carried out with an aim to improve the mechanical properties of PHB by blending PHB with PHBV, which is more flexible and processable than PHB (Gassner *et al.*, 1996). The stiffness of PHB and PHBV could be overcome via formation of an ultrafine fibrillar structure. Ultrafine fibrous structures have a high surface-to-volume ratio which is generally thought to enhance cell adhesion. Due to the dependence of cell migration, proliferation and differentiated function on cell adhesion, these ultrafine fibrous structures could improve these biological functions. Such an ultrafine fibrous matrix could be formed by three methods that are self-assembly, phase-separation and electrospinning. Electrospinning

seems to be the only method which can be further developed for mass production of one-by-one continuous nanofibers from various polymers. Moreover, the advantages of electrospinning process are simple equipment and producing fibers with an ability of controlling the orientation, size, and the thickness of the as-spun mats.

#### 4.1 Electrospinning of PHB and PHBV Solutions

Table 4.1 summarizes viscosity and electrical conductivity (raw data are shown in Appendix A) of the as-prepared PHB and PHBV solutions in chloroform at various concentrations ranging between 10 and 16% w/v. Even though the molar mass of PHBV is about twice that of PHB, the viscosity of PHBV solution at a given concentration was slightly lower than that of PHB counterpart. With regards to the electrical conductivity of the as-prepared PHB solutions, variation in the solution concentration did not affect much the property value of the solutions, while, for that of the as-prepared PHBV solutions, a slight increase in the property value with increasing solution concentration was observed. Comparatively, at 10 and 12% w/v, the electrical conductivity of the PHBV solutions was slightly lower than that of the PHB counterparts, while, at 16% w/v, it was slightly greater.


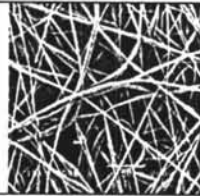
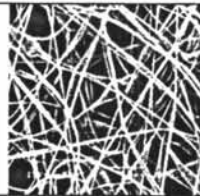





**Table 4.1** Viscosity and conductivity of the as-prepared PHB and PHBV solutions at 25°C as a function of concentration

Solution concentration (wt.%)	Viscosity (cP)		Electrical conductivity ( $\mu\text{S}\cdot\text{cm}^{-1}$ )	
	PHB	PHBV	PHB	PHBV
10	435	328	$0.063 \pm 0.006$	$0.053 \pm 0.006$
12	710	585	$0.070 \pm 0.000$	$0.063 \pm 0.006$
14	1394	1081	$0.070 \pm 0.000$	$0.070 \pm 0.000$
16	2333	1555	$0.070 \pm 0.000$	$0.077 \pm 0.006$

In order to optimize the collection distance that resulted in the as-spun fibers with optimized diameters and areal density, 14% w/v PHB solution in chloroform was electrospun under an applied electrical potential of 12 kV for 5 min. With increasing collection distance, the average diameter of the as-spun fibers was found to monotonously decrease from about 8.0  $\mu\text{m}$  at the collection distance of 15 cm to about 3.8  $\mu\text{m}$  at the collection distance of 25 cm, while the areal density was found to reach a maximum at the collection distance of 20 cm (results not shown). Increasing collection distance for a fixed applied electrical potential translates to decreased electrostatic field strength, hence decreased electrostatic forces exerting on a jet segment. The decreased electrostatic forces cause the jet to exhibit the bending instability closer to the nozzle tip, resulting in the actual trajectory of the jet to increase appreciably (i.e. the looping trajectory) (Reneker, 2000; Mit-uppatham, 2004). The increased path trajectory with increasing collection distance allows the jet to elongate and thin down in a greater extent prior to solidifying.

Table 4.2 shows selected SEM images of as-spun products from 10 and 14% w/v PHB solutions that were spun under an electrical potential of 8 to 14 kV over a fixed collection distance of 20 cm. Though not shown, 12 and 16% w/v PHB solutions and 10 – 16% w/v PHBV solutions were also electrospun under the same condition. Beaded fibers were obtained from PHB solutions with concentration lower than 14% w/v as well as 14% w/v PHB solution that was spun at low applied electrical potentials (i.e. 8 – 10 kV) and PHBV solutions with concentration lower than 12% w/v as well as 12% w/v PHBA solution that was spun at 8 kV. For a given applied electrical potential and a given polymer, increasing concentration of the spinning solution caused the diameters of the fibers to increase. In the case where beaded fibers were obtained, increasing concentration of the spinning solution caused the tendency for bead formation to decrease. For a given concentration and a given polymer, increasing applied electrical potential caused the fiber diameters to increase and the bead size to decrease. Slight discrepancy from the aforementioned observation should be a result of certain complications during electrospinning, e.g. partial clogging of the spinning solution at the tip of the nozzle that contributed to the inconsistency in the flow of the solution.

**Table 4.2** Selected SEM images (scale bar = 50  $\mu\text{m}$  and magnification = 500x) illustrating the effect of applied electrical potential and solution concentration on morphology of fibers that were electrospun from PHB solutions in chloroform as well as average values of fiber diameters, bead sizes, number of fibers per unit area (i.e. fiber density) and number of beads per unit area (i.e. bead density). The collection distance was fixed at 20 cm

Concentration (% w/v)	Applied potential (kV)				
	8	10	12	14	
10					
	Fiber diameters( $\mu\text{m}$ )	$1.6 \pm 0.3$	$2.8 \pm 0.6$	$2.9 \pm 0.6$	$3.5 \pm 0.9$
	Bead size( $\mu\text{m}$ )	$11.2 \pm 4.9$	$7.0 \pm 2.2$	$9.7 \pm 3.7$	$8.1 \pm 3.2$
	Fiber density ( $\times 10^{-2} \# \cdot \mu\text{m}^{-2}$ )	$14.5 \pm 2.6$	$65.4 \pm 5.3$	$65.9 \pm 3.7$	$24.3 \pm 2.3$
	Bead density ( $\times 10^{-2} \# \cdot \mu\text{m}^{-2}$ )	$30.5 \pm 6.2$	$30.1 \pm 1.7$	$38.7 \pm 4.6$	$18.5 \pm 6.0$
14					
	Fiber diameters( $\mu\text{m}$ )	$4.1 \pm 1.0$	$4.4 \pm 0.9$	$4.3 \pm 1.0$	$6.6 \pm 1.0$
	Bead size( $\mu\text{m}$ )	$8.0 \pm 2.8$	$8.5 \pm 2.6$	-	-
	Fiber density ( $\times 10^{-2} \# \cdot \mu\text{m}^{-2}$ )	$35.4 \pm 8.7$	$31.6 \pm 3.7$	$40.2 \pm 1.6$	$35.7 \pm 8.1$
	Bead density ( $\times 10^{-2} \# \cdot \mu\text{m}^{-2}$ )	$10.7 \pm 3.3$	$9.8 \pm 2.2$	-	-

At low concentrations of the spinning solutions, surface tension is the dominant factor. In such circumstances, either only electrospayed beads or beaded fibers were formed. Above a critical value of the concentration, electrospun fibers as a non-woven mat on the collector were obtained. For a given applied electrical

potential, increasing concentration caused the ejected, charged jet to travel in a straight trajectory prior to the onset of the bending instability in a much longer distance. This causes the total path trajectory of the jet to decrease, hence the less tendency for the jet to be elongated and thinned down before depositing on the collector (Reneker, 2000; Mit-uppatham, 2004). For a given concentration, increasing applied electrical potential not only shifted the onset of the bending instability towards the collector, it also caused the material flowrate from the tip of the nozzle to increase, both as a result of the increase in the electrostatic forces (Mit-uppatham *et al.*, 2004). Both phenomena should attribute to the observed increase in the fiber diameters with increasing applied electrical potential. However, such an explanation is only applicable when multiple jetting was not observed. We also observed that, under a very high applied electrical potential, the occurrence of the multiple jetting produced uncharacteristic decrease in the fiber diameters and this could be a reason for the observed increase and subsequent decrease in the fiber diameters with increasing applied electrical potential (Buchko *et al.*, 1999).

In all of the spinning conditions investigated, the average diameter of the as-spun PHB fibers ranged between 1.6 and 8.8  $\mu\text{m}$ , while that of the as-spun PHBV fibers ranged between 1.6 and 4.7  $\mu\text{m}$ . In addition, among the various spinning conditions investigated, 14% w/v solutions at the applied electrical potential of 12 kV were chosen as the condition to further study the electrospinning of PHB/PHBV blends.

## 4.2 Electrospinning of PHB/PHBV Solutions

Table 4.3 summarizes viscosity and electrical conductivity of the as-prepared PHB/PHBV solutions in chloroform at various weight compositions between PHB and PHBV. The total concentration of the solutions was 14% w/v. Apparently, the viscosity of the solutions decreased monotonously from that of the pure PHB solution (i.e. 1394 cP) to that of the pure PHBV solution (i.e. 1081 cP). Interestingly, despite the fact that both the pure PHB and the pure PHBV solutions exhibited a similar electrical conductivity value, blending of both the pure solutions


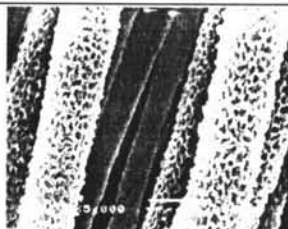
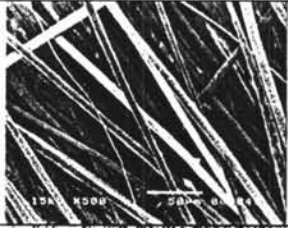
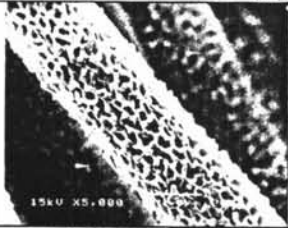

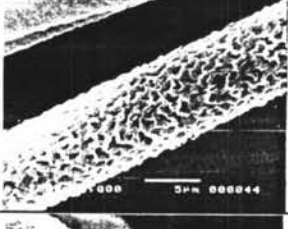



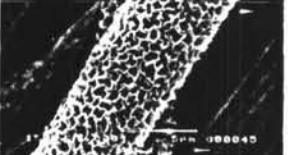
caused the electrical conductivity to increase and, at the solution containing equal amount of both polymers, the electrical conductivity was a maximum. The reason for such an observation is not certain at this point.

**Table 4.3** Viscosity and conductivity of the as-prepared PHB/PHBV blend solutions at 25°C as a function of blend composition. The concentration of the blend solutions was 14 wt.%

Blend composition (PHB/PHBV w/w)	Viscosity (cP)	Electrical conductivity ( $\mu\text{S}\cdot\text{cm}^{-1}$ )
100/0	1394	$0.070 \pm 0.000$
75/25	1302	$0.087 \pm 0.006$
50/50	1252	$0.093 \pm 0.006$
25/75	1167	$0.077 \pm 0.006$
0/100	1081	$0.070 \pm 0.000$

Electrospinning of these solutions was carried out under an applied electrical potential of 12 kV over a fixed collection distance of 20 cm on a rotating cylindrical drum which was set to rotate at 1000 rpm. Selected SEM images at two different magnifications as well as average value of the fiber diameters are summarized in Table 4.4. Apparently, rather well-aligned, cross-sectionally-round fibers without the presence of beads were obtained at all weight compositions investigated. The SEM images with the higher magnification show that the surface of the as-spun fibers was very rough. It is postulated that such surface roughness was a result of the rapid phase separation that occurred during rapid evaporation of the solvent when a highly volatile liquid was used as the solvent (viz. the boiling point of chloroform = 61.3°C). While the polymer-rich phase formed a part of the fiber matrix, the solvent-rich phase gave rise to the formation of surface indentations. Recently, it was demonstrated that both the relative humidity and solvent evaporation contributed to the formation of indentations on the surface of electrospun polystyrene fibers.

**Table 4.4** Selected SEM images illustrating the effect of blend composition on morphology of fibers that were electrospun from PHB, PHBV, and PHB/PHBV solutions in chloroform as well as average values of fiber diameters. The solution concentration was 14% w/v. The applied electrical potential, the collection distance, and the angular velocity of the drum collector were 12 kV, 20 cm, and 1000 rpm, respectively

Blend composition (PHB/PHBV w/w)	Magification		Fiber diameters ( $\mu\text{m}$ )
	500x	5 000x	
100/0			$3.7 \pm 1.7$
75/25			$3.3 \pm 1.7$
50/50			$4.0 \pm 1.1$
25/75			$3.2 \pm 1.3$
0/100			$2.3 \pm 2.1$

With regards to the size of the fibers, it is interesting that the average diameter of the as-spun fibers from PHB/PHBV blend solutions was larger than those of the as-spun fibers from pure polymer solutions (i.e. 3.7  $\mu\text{m}$  for as-spun PHB fibers and 2.3  $\mu\text{m}$  for as-spun PHBV fibers), especially for the as-spun fibers from 50:50 PHB/PHBV blend solution that exhibited the greatest average diameter value (i.e. 4.0  $\mu\text{m}$ ). This is quickly recognized as a result of the greatest electrical conductivity that the 50:50 PHB/PHBV blend solution exhibited (see Table 4.3). The greatest electrical conductivity leads to the greatest electrostatic forces exerting on a jet segment, leading to decreased total path trajectory and/or increased material flow rate, as previously mentioned. For further investigation, these pure and blend solutions were electrospun continuously for either 8 or 12 h to produce as-spun fiber mats with thickness of about  $85 \pm 5$  and  $105 \pm 5$   $\mu\text{m}$ , respectively.

#### 4.2.1 Thermal and Physical Properties

Thermal properties of the as-spun pure and blend fibers including those of the as-received resins were investigated by DSC and TGA. In DSC, the objective for each cooling or heating run is as follows: HEAT1 is to observe the melting behavior of the original crystalline entity of each sample; COOL is to observe the ability of the sample to crystallize when it was subjected to a constant cooling scan; and HEAT2 is to observe the melting behavior of the crystalline entity of the sample which was formed during the cooling scan. Experimental values for all of the DSC and TGA analyses are summarized in Table 4.5.

In the first heating (HEAT1), the apparent melting temperature ( $T_{m,o}$ ) of the as-received PHB and PHBV powder was observed at 172.6 and 158.7°C, respectively. Similarly,  $T_{m,o}$  value of the as-spun PHB and PHBV fibers was observed at 173.1 and 162.3°C, respectively. For the as-spun PHB/PHBV fibers,  $T_{m,o}$  value was found to decrease with increasing PHBV content. Since PHBV is less crystallizable than PHB (due to the presence of the non-crystallizable comonomer units of about 5% by mole), blending PHB with PHBV caused both the apparent melting temperature and the crystallinity to decrease. With regards to the crystallinity, the apparent enthalpy of fusion ( $\Delta H_f$ ) as obtained from HEAT1 was used to calculate



the apparent degree of crystallinity ( $\chi_{c,PHB}^{DSC}$ ). Clearly,  $\chi_{c,PHB}^{DSC}$  was found to be a decreasing function of the PHBV content.

**Table 4.5** Thermal characteristics and apparent crystallinity of as-spun PHB, PHBV, and PHB/PHBV fiber mats of about  $85 \pm 5 \mu\text{m}$  thick as well as those of PHB and PHBV powder

Blend composition (PHB/PHBV w/w)	$T_g^a$ (°C)	$T_{m,o}^a$ (°C)	$T_{mc}^a$ (°C)	$T_{cc}^a$ (°C)	$T_{m,s}^a$ (°C)	$\Delta H_f^a$ (J·g <sup>-1</sup> )	$T_d^b$ (°C)	$\chi_{c,PHB}^{DSC}$ (%) <sup>c</sup>
100/0	-	173.1	89.9	-	155.1, 165.4	81.5	265.0	55.6
75/25	-	172.2	71.6	-	144.8, 159.1	80.6	263.6	55.0
50/50	-	167.4	81.3	-	153.5, 165.0	74.7	265.0	51.0
25/75	-	167.0	77.3	-	151.8, 162.8	70.6	265.0	48.2
0/100	-	162.3	79.0	-	152.8, 163.8	66.1	265.3	45.1
PHB powder	-	172.6	86.7	-	149.3, 162.8	77.8	263.5	53.1
PHBV powder	~0	158.7	54.4 <sup>d</sup>	54.4	150.5, 163.6	75.9	265.5	51.8

<sup>a</sup> These data were determined by DSC:  $T_g$ , glass transition temperature, obtained from HEAT2;  $T_{cc}$ , cold-crystallization peak temperature, obtained from HEAT2;  $T_{m,o}$ , apparent melting peak temperature of the original samples, obtained from HEAT1;  $T_{m,s}$ , apparent melting peak temperature of the samples subjected to second heating, obtained from HEAT2; and  $\Delta H_f$ , apparent enthalpy of fusion, obtained from HEAT1.

<sup>b</sup>  $T_d$ , thermal degradation temperature, determined by TGA.

<sup>c</sup>  $\chi_{c,PHB}^{DSC}$ , apparent degree of crystallinity, calculated from  $\Delta H_f / \Delta H_f^0$  (i.e.  $\Delta H_f^0 = 146.6 \text{ J}\cdot\text{g}^{-1}$ ).

<sup>d</sup> a very broad exotherm.

In the subsequent cooling (COOL), the as-received PHB powder exhibited the crystallization peak temperature ( $T_{mc}$ ) at 86.7°C, while the as-received PHBV powder showed a very broad peak centering at 54.4°C. Clearly, the presence of the HV comonomer of about 5% by mole was enough to inhibit the crystallization of PHBV during cooling appreciably. Interestingly, the as-spun PHBV fibers exhibited the  $T_{mc}$  value at 79.0°C, which is much higher than that of the as-received powder, while the as-spun PHB fibers exhibited a similar value (i.e. 89.9°C) to that of the as-received powder. The observed greater  $T_{mc}$  value of the as-spun PHBV fibers over that of the as-received powder was postulated to be a result of certain degree of molecular orientation that was not completely relaxed during melt-annealing at 195°C for 2 min. Insufficient melting was shown to affect the subsequent crystallization behavior of preoriented poly(trimethylene terephthalate) (PTT) samples considerably (Supaphol *et al.*, 2004). Unexpectedly, the as-spun blend fibers containing 25 wt.% PHBV exhibited the lowest  $T_{mc}$  value at 71.6°C, while those containing 50 and 75 wt.% PHBV exhibited the  $T_{mc}$  values at 81.3 and 77.3°C, respectively.

In the subsequent heating (HEAT2), only the as-received PHBV powder exhibited a cold crystallization peak ( $T_{cc}$ ) at 54.4°C, since it only partially crystallized during previous cooling at 10°C·min<sup>-1</sup>. In addition, it was the only sample that exhibited a glass transition temperature ( $T_g$ ) at about 0°C, due to the high amorphous content of the sample. For all samples, double melting phenomenon was evident. As in the case of PTT (Srimoan *et al.*, 2004), the occurrence of the lower melting endotherm corresponded to the melting of the primary crystallites formed during previous cooling, while that of the higher melting endotherm corresponded to the melting of the recrystallized crystallites formed during subsequent heating scan. All of the samples exhibited the low melting endotherm in the range of 144.8 – 153.5°C, with that of the as-spun fibers containing 25 wt.% PHBV exhibiting the lowest value at 144.8°C, which corresponded to the lowest  $T_{mc}$  value that this sample exhibited.

Thermal degradation of these samples was also investigated. Though not shown, these samples exhibited one step in the loss of their weight centering about 263.6 – 265.5°C. The wettability of both the fiber mat and corresponding film

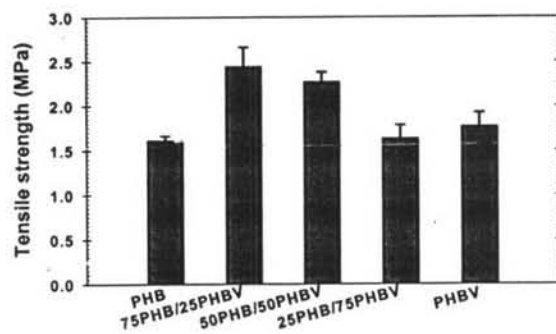
surfaces was assessed by evaluating the contact angle of a sessile droplet of distilled water on these surfaces. The results are summarized in Table 4.6 and the raw data are shown in Appendix B. Evidently, all of the fiber mat samples exhibited the water contact angle in the range of about 156 - 122°, while all of the film counterparts showed the value in the range of about 68 - 77°. The observed hydrophobicity of the fiber mats in comparison with that of the films should be a result of the surface roughness that introduced multiple contacting points on the water surface such that the interface between the water droplet and the fiber mat surface was not exactly solid/liquid.

**Table 4.6** Static contact angle of distilled water on surfaces of as-spun PHB, PHBV, and PHB/PHBV fiber mats of about  $105 \pm 5 \mu\text{m}$  thick

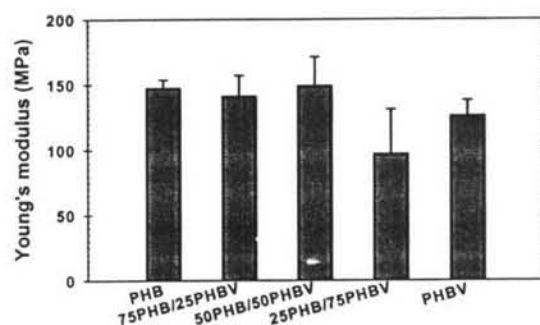
Blend composition (PHB/PHBV w/w)	Static contact angle (degrees)
As-spun fiber mats	
100/0	$115.5 \pm 3.4$
75/25	$118.5 \pm 2.0$
50/50	$121.4 \pm 2.2$
25/75	$121.6 \pm 1.7$
0/100	$117.5 \pm 2.5$
As-cast films	
100/0	$68.0 \pm 2.1$
75/25	$74.9 \pm 2.2$
50/50	$75.2 \pm 4.0$
25/75	$76.8 \pm 2.0$
0/100	$73.4 \pm 2.3$

#### 4.2.2 Mechanical Integrity

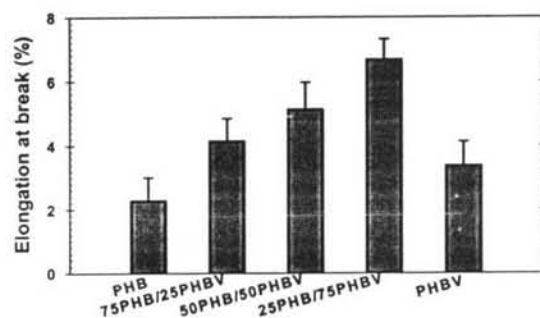
Mechanical properties, in terms of the tensile strength, Young's modulus, and elongation at break, of both the as-spun pure and blend fiber mats were investigated and the results are illustrated in Figure 4.1. The tensile strength of the as-spun PHB and PHBV fiber mats was found to be quite comparable (i.e. 1.6 and 1.8 MPa, respectively). Clearly, all but one of the as-spun PHB/PHBV fiber mats exhibited the tensile strength greater than those of the pure ones. Interestingly, all of the as-spun blend fiber mats exhibited much greater elongation at break than those of the pure ones and, with increasing PHBV content, the elongation at break of the blend fiber mats was found to increase. Lastly, Young's modulus for the as-spun PHB fiber mat and the as-spun blend fiber mats containing 25 and 50 wt.% PHBV was very similar (i.e. 147 – 149%), which was greater than those of the as-spun PHBV fiber mat and the as-spun blend fiber mat containing 75 wt.% PHBV, respectively.



(a)



(b)



(c)

**Figure 4.1** Mechanical properties of fiber mats of about  $105 \pm 5 \mu\text{m}$  thick that were electrospun from PHB, PHBV, and PHB/PHBV solutions in chloroform. The solution concentration was 14% w/v. The applied electrical potential, the collection distance, and the angular velocity of the drum collector were 12 kV, 20 cm, and 1000 rpm, respectively. Raw data are shown in Appendix C.

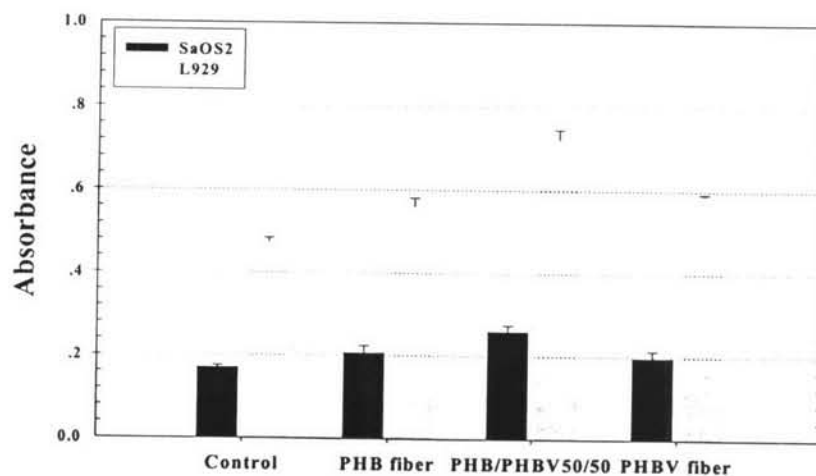
### 4.3 Cell Study

The cast film and electrospun fibrous scaffolds of PHB, PHBV and their blends containing 50wt% PHBV scaffold—prepared from 14%(w/v) electrospinning solutions—were used for cytotoxicity test, cell attachment, and cell proliferation measurements (Raw data were shown in Appendix D).

#### 4.3.1 Indirect Cytotoxicity Test

In the electrospinning of PHA solution to prepare mats to be used as scaffolds for tissue engineering applications, chloroform is the preferred solvent. In this way, residual amounts of organic solvents associated with the fibers should be avoided and can be possible problems related to the interaction between the organic solvent and seeded cells. To confirm that all of the PHA scaffolds were not toxic to viable cells, cytotoxicity test was carried out.

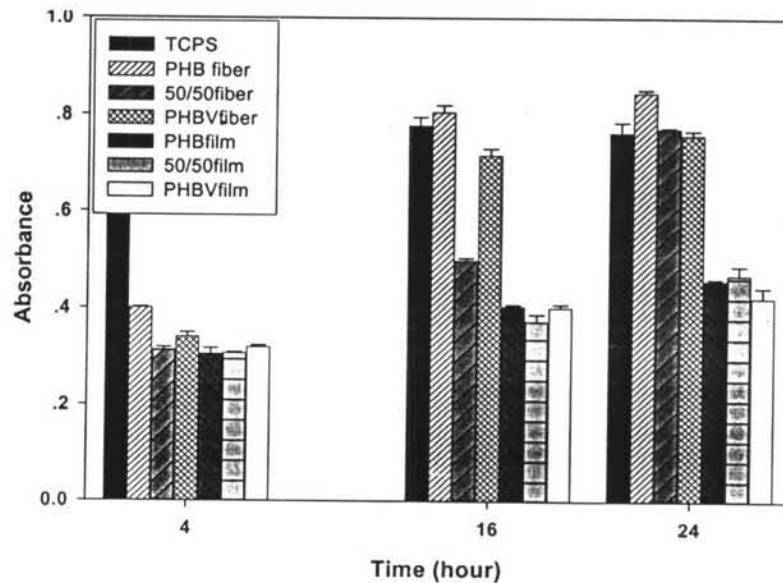
Fibrous scaffolds were seeded with human osteoblasts, SaOS2, and mouse fibroblasts, L929. To abide by with the ISO10993-5 standard test method, cytotoxicity evaluation with L929 cells was necessary.



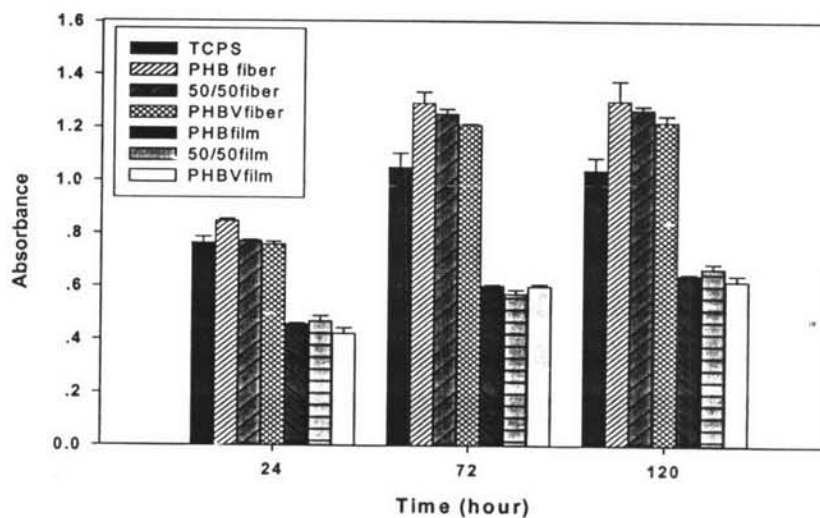
**Figure 4.2** Indirect cytotoxic evaluation of fibrous scaffolds from electrospun mats of PHB and PHBV and their blend fibers based on viability of human osteoblasts (SaOS2) and mouse fibroblasts (L929).

Figure 4.2 demonstrates that the absorbance obtained from MTT assay of the cells which were cultured with the extraction media in comparison with those cultured with SFM as a control for this study. The MTT assay is a method that quantifies the amount of purple formazan crystals formed when MTT reacted with mitochondrial enzyme of living cells and is proportional to the number of viable cells. All of the fibrous scaffolds exhibited much greater average absorbance values with L929 cells compared with those with SaOS2 cells. Furthermore, it was found that PHB, PHBV, PHB/PHBV fibrous scaffolds exhibited higher average absorbance value with both types of cells, in comparison with those of the control. This suggests that these fibrous materials were non-toxic to both types of cells and could be useful as scaffolds for bone regeneration.

#### 4.3.2 Cell Attachment and Proliferation



**Figure 4.3** Attachment of SaOS2 on TCPS, films and fibrous scaffolds as a function of time in culture.



**Figure 4.4** Proliferation of SaOS2 on TCPS, films and fibrous scaffolds as a function of time in culture.

A tissue-engineered scaffolding material must support cellular attachment and growth. To evaluate cellular behavior on film and fibrous scaffolds of PHB, PHBV and 50PHB/50PHBV, SaOS2 cells were seeded and cultivated on those scaffolds in wells of a 24-well plate. After 4 h in culture, the viability of the cultured cells on any type of both the film and the fibrous scaffolds was much less than that on TCPS (Figure 4.3), possibly due to the low hydrophilicity of the material. It appeared that an appropriate combination of hydrophilicity and hydrophobicity was important for the biocompatibility of PHA, especially for the attachment of SaOS2 cells on the surface of these materials (Thomas *et al.*, 1985). Also the irregularity of the surface morphology interfered the attachment of cells on the materials. After longer culturing times (i.e., 16 h and 24 h), the viability of SaOS2 on the fibrous scaffolds was much improved when compared with that on TCPS and it was much greater than that on the film scaffolds. Qualitatively, the viability of cells on the fibrous scaffolds after 24 h in culture can be ranked as follows: PHB > 50PHB/50PHBV  $\approx$  PHBV.

Proliferation evaluation of SaOS2 cells cultured on TCPS and both the film and the fibrous scaffolds after 24, 72, and 120 h in culture by MTT assay. The viability of the cells on various types of scaffolds and TCPS at the end of each

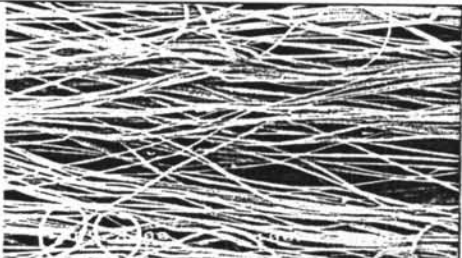

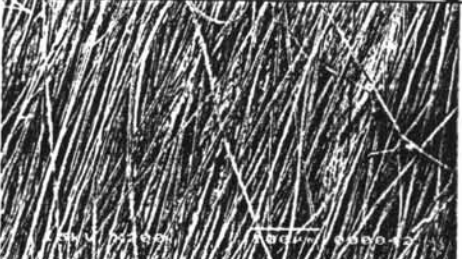





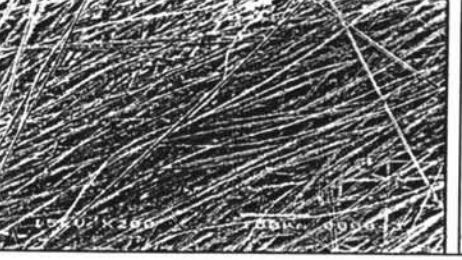



culture period is shown in Figure 4.4. After 24 h in culture, the viability of the SaOS2 on all of the fibrous scaffolds was comparable to that on TCPS and was much greater than that on all of the film scaffolds. After long culture times (i.e., 72 and 120 h), the viability of the cells on all of the fibrous scaffolds was distinctively greater than that on TCPS and was even much greater than that on all of the film scaffolds. Interestingly, the viability of the cells on all of the substrates after 72 and 120 h in culture appeared to be quite similar. The saturation in the viability of the cells could be a result of the differentiation of the cells. In addition, the likely explanation for the observed increase in the viability of the cells after long culture times on all of the fibrous scaffolds could be the highly porous nature of the scaffolds that provided large surface area onto which cells could propagate.

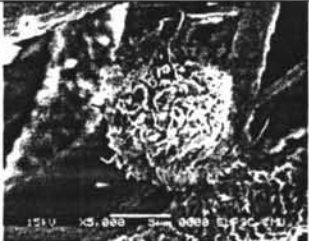
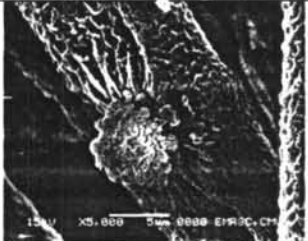


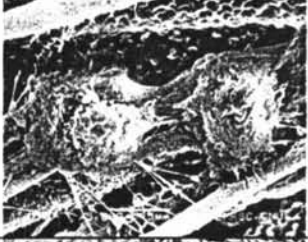
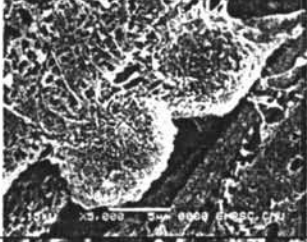




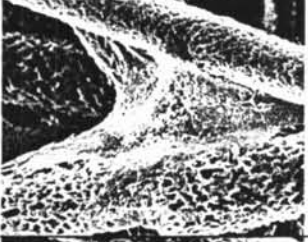
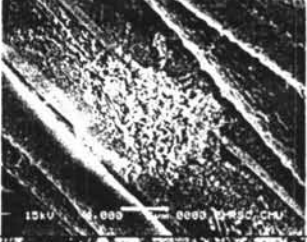
Table 4.7 shows selected low-magnification SEM images (200x and scale bar = 100  $\mu\text{m}$ ) of SaOS2 that were cultured on 50PHB/50PHBV fibrous scaffold at different times in culture (i.e., 4, 16, 24, 72, and 120 h). Selected SEM images of neat as-spun scaffolds after submersion in culture medium at the same time in culture are also illustrated in Table 4.7. Clearly, the fibrous scaffolds retained their fibrous structure even after submersion in the culture medium for as long as 120 h. It should be noted that the reason that the SEM images of cell-cultured PHB and PHBV fibrous scaffolds were not shown were due to the similarity to those shown in Table 4.7. Despite the observed increase in the cell viability after different times in culture (see Figures 4.3 and 4.4), such an increase could not be observed in these SEM images shown here. A possible reason was that, due to the relatively large pore sizes of the fibrous scaffolds, the cells could very well penetrate into the inner side of the scaffolds. Selected SEM images of higher magnification (5000x and scale bar = 5  $\mu\text{m}$ ) are shown in Table 4.8. Clearly, during the first 4 h in culture (attachment stage), the morphology of the cells was largely in round shape with slight trace of filopodia. After 16 h in culture, division of cells was evident on all types of the fibrous scaffolds. At longer culture times (i.e., 24 to 120 h), the cells on all types of the fibrous scaffolds expanded even more, with an evidence of the anchoring ligands reaching out to help support them on the fiber surface. According to the results obtained, all types of the fibrous scaffolds from PHA, PHBV, and PHB/PHBV appeared to support both the attachment and the proliferation of SaOS2 particularly

well, the results indicating the potential for use of these fibrous mats as bone scaffolds.

**Table 4.7** Selected SEM images SaOS2 cultured on fibrous PHB/PHBV (50wt%PHBV) blend scaffolds at different times in culture (Scale bar = 100  $\mu$ m.)

Time in culture (hr)	As-spun PHB/PHBV 50/50	PHB/PHBV 50/50 + SaOS2 cells
4		
16		
24		
72		
120		

**Table 4.8** Selected SEM images SaOS2 cultured on various types of PHA scaffolds at different times in culture (Scale bar = 5  $\mu$ m.).

Time in culture (hr)	Substrates		
	PHB	PHB/PHBV 50/50+SaOS2	PHBV
4			
16			
24			
72			
120	